Proceedings of the ASME 2009 International Manufacturing Science and Engineering Conference
MSEC2009
October 4-7, 2009, West Lafayette, Indiana, USA

MSEC2009-84364

SHAPE MEMORY PROPERTY ALTERATION OF AMORPHOUS NITI THIN FILMS THROUGH AGING HEAT TREATMENT

Gen Satoh, Andrew Birnbaum, Y. Lawrence Yao
Columbia University
Department of Mechanical Engineering
New York, NY, USA

ABSTRACT

Thin film shape memory alloys have recently become a promising material for actuation of devices on the micro scale such as micro-pumps and micro-valves. Their utilization, however, has been limited due to the difficulty in tailoring their properties for different applications. Control over the transformation temperatures as well as mechanical and shape memory properties is required to enable their widespread use. This study examines the effects of heat treatment time and temperature on the properties of amorphous, Ti-rich NiTi thin films on silicon substrates. The effects on the transformation temperatures are investigated through the use of temperature dependent optical microscopy. The modulus and hardness, as well as dissipated energy and depth recovery are obtained through nano-indentation and atomic force microscopy (AFM). The role of microstructure and composition in altering both the mechanical and shape memory properties of the films is discussed.

INTRODUCTION

Originally observed in bulk specimens, the shape memory effect (SME) and superelasticity (SE) are characteristics shared by the class of materials called shape memory alloys (SMA). These materials generated a great deal of interest in their infancy due to their ability to recover large deformations upon heating and endure significant, seemingly elastic strains. Their widespread use, however, was hampered by their slow response times due to their large thermal mass and difficulties controlling the transformation temperatures of the material. Recently, thin-film shape memory alloys have gained popularity due to their small thermal mass and thus fast response time, and are of particular interest for use in micro electromechanical devices (MEMS) as actuators due to their ability to produce large forces and displacements. One particular SMA, NiTi, has been the focus of extensive research for biomedical applications due to its excellent biocompatibility and good shape memory characteristics. NiTi thin films have been applied to various MEMS applications such as micro-grippers and micro-valves [1].

Crystallization of the amorphous thin films produced through sputtering is typically performed by furnace annealing. Furnace annealing of thin film specimens has been shown to produce specimens that exhibit shape memory properties comparable to those of bulk materials [2]. Lee et. al [3] have characterized the nucleation and growth of NiTi crystals in amorphous sputtered films through in-situ TEM observation. Furthermore, control over transformation temperature, recoverable strain, and even biocompatibility have been demonstrated by varying annealing parameters and deposition conditions [4-6].

X-ray diffraction (XRD) and transmission electron spectroscopy (TEM) among others have been the primary methods by which both bulk and thin film SMA have been characterized. These methods have been used to determine the crystal structure, phase transformation temperatures, and precipitation behavior of annealed specimens. The increased interest in thin film SMA also requires the use of different characterization methods that can accurately test materials in this form. Recent studies of the micro and nano-scale properties of SMA such as NiTi have made use of nanoindentation for this purpose. Gall et. al [7] have studied the nanoindentation response of bulk, Ni-rich, superelastic, single crystal NiTi in different orientations. Nanoindentation of thin films has also been used to determine the mechanical properties of sputtered and annealed films as a function of composition and film thickness [8,9]. Nanoindentation is particularly appealing for thin film specimens since they are not easily characterized by conventional means. There remains to be, however, a systematic study on the effects of heat treatment, specifically temperature and dwell time, on the nanoindentation response of thin film Ti-rich NiTi.

In this study, the effects of aging heat treatments on amorphous, sputtered, Ti-rich NiTi films are examined to provide insight into the evolution of their microstuctures and shape memory properties. Specifically, the effects of annealing temperature and dwell time on the transformation temperatures and mechanical and shape memory properties are characterized through the use of optical microscopy, nanoindentation, and atomic force microscopy measurements.

BACKGROUND

Shape Memory and Superelasticity

The shape memory effect (SME) and superelasticity (SE) exhibited by shape memory alloys are both manifestations of a reversible crystallographic shift called the martensitic transformation. For NiTi, the high-temperature or parent phase, austenite, has a cubic (β_2) structure and is ordered like CsCl. The low-temperature phase, martensite, has a monoclinic structure which is achieved through a shear-like deformation of the parent lattice. Thermodynamically, the driving force for the transformation is the change is free energy between the austenite and martensite structures where the free energy for each phase can be written as [10]

$$G^* = U + PV - TS - Fl = H^* - TS \qquad (1)$$

where U, P, V, T, S, F, and l are the internal energy, pressure, volume, temperature, entropy, force applied to the specimen, and length of the specimen respectively. The enthalpy component of the free energy is denoted H^*. At the equilibrium temperature the free energy of martensite is equal to that of the austenite. Additionally, the changes in the free energies of the phases are equal which gives the following relation at constant pressure

$$\begin{aligned} dG^{*A} = dG^{*M} &= -S^A dT - l^A dF \\ &= -S^M dT - l^M dF \end{aligned} \qquad (2)$$

where the superscripts 'A' and 'M' indicate the values for austenite and martensite respectively. Therefore, at the equilibrium temperature and constant pressure

$$\frac{d\sigma}{dT} = -\frac{\Delta S^{A\to M}}{\varepsilon^{A\to M}} = -\frac{\Delta H^{*A\to M}}{T_o(\sigma)\varepsilon^{A\to M}} \qquad (3)$$

Equation 3 is the Clausius-Clapeyron relationship for stress and temperature for the phase transition between austenite and martensite and quantifies the change in the equilibrium temperature, T_o, with applied stress and conversely, changes in the stress required to induce the phase transformation with changes in the equilibrium temperature. The power of this relationship is most clearly seen in Fig. 1, which is a schematic phase diagram of NiTi in the stress-temperature domain. Here, Eq. 3 is used to define the slope of the lines delineating the phase regions.

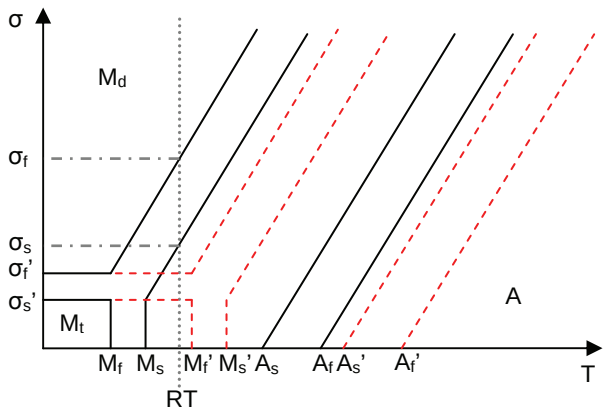

FIGURE 1: SCHEMATIC DIAGRAM OF THE STRESS-TEMPERATURE PHASE DIAGRAM FOR NITI.

As shown in Fig. 1, a shift in the transformation curves from a material with transformation temperatures M_f, M_s, A_s, and A_f (solid lines) to a material with higher transformation temperatures M_f', M_s', A_s', and A_f' (dashed lines) is accompanied by a decrease in the critical stresses for transformation at room temperature from σ_s and σ_f to σ_s' and σ_f'. σ_s and σ_f denote the stresses required to start and finish the transformation from austenite or twinned martensite to de-twinned martensite respectively. The stress-temperature phase diagram is essential to understanding the mechanical response of NiTi devices and its sensitivity to the transformation temperatures of the material. For example, for the simplest case of uniaxial loading of a SMA device in an isothermal environment, the load path is characterized by traveling vertically within the stress-temperature phase diagram with phase transformations indicated by crossing the delineating lines. Upward shifts in the transformation temperatures of the material results in decreased stress required to induce the transformation while downward shifts in transformation temperatures results in an increased critical stress for transformation.

For simplicity we define the critical stress to induce the phase transformation as a single value, σ_{mr}. While the value of the critical stress is not always of great importance, its relationship to the yield stress, σ_Y, defines the material response of SMA devices. Materials with $\sigma_{mr} > \sigma_Y$ will exhibit a conventional elastic-plastic response with no shape memory or superelastic properties. Since the yield stress is below the critical stress, deformation will be accommodated by plasticity before any phase transformation takes place. Materials with $\sigma_{mr} < \sigma_Y$ will undergo a phase transformation upon loading before reaching plasticity and, depending on the transformation temperatures at zero stress, will exhibit shape memory or superelastic properties.

Indentation and Depth Recovery

Under more complex loading conditions such as those caused by indentation, a mixture of deformation accommodated by phase transformation and deformation accommodated by plasticity is typically seen due to non-uniform stress distributions in the material. Modeling of this process begins with Hill [11] who used an expanding cavity

model to determine the radial displacement, *u(r)*, of material surrounding an expanding hemi-spherical cavity.

$$u(r) = \frac{Y_{pl} r}{E}\left[(1-\upsilon)\frac{{c_{pl}}^3}{r^3} - \frac{2}{3}(1-2\upsilon) - 2(1-2\upsilon)ln\left(\frac{c_{pl}}{r}\right)\right] \quad (4)$$

where Y_{pl} is the yield stress, E is Young's modulus, c_{pl} is the radius of the elastic-plastic interface, and υ is Poisson's ratio. Johnson [12] applied this model to the displacements produced by a conical indenter which have been shown to be radial with contours being roughly hemi-spherical in shape. Taking the derivative of Eq. (4) with respect to c and conserving volume as the indenter tip is pushed into the material as

$$2\pi a^2 du(a) = \pi a^2 dh = \pi a^2 tan(\beta) da \quad (5)$$

where, due to the geometry of the cone indenter tip, $dc/da = c/a = const$, the radius of the plastically deformed region can be defined as

$$c_{pl} = \frac{d}{\tan\beta}\left[\frac{E\tan\beta}{6Y_{pl}(1-\upsilon)} + \frac{2-4\upsilon}{3-3\upsilon}\right]^{1/3} \quad (6)$$

where d is the indentation depth and β is the angle between the indenter face and the film surface (19.7° for the equivalent cone for a berkovich indenter). Similarly, by replacing Y_{pl} with Y_{mr}, the critical stress to induce de-twinning of martensite, the radius of the shape memory region, c_{mr}, can be determined. Following Shaw et. al. [13], since only the material within the shape memory region and outside the plastic region recovers when heated, assuming twinned and de-twinned martensite have the same modulus and Poisson's ratio, the theoretical depth recovery ratio, R_{th}, of a martensitic film under indentation by a conical indenter tip can be determined and is written as

$$R_{th} = \frac{c_{mr} - c_{pl}}{c_{mr}} \approx 1 - \left(\frac{Y_{mr}}{Y_{pl}}\right)^{1/3} \quad (7)$$

This relationship illustrates the importance of these critical stresses on the material response of the films. Unlike the uniaxial loading case, under indentation by a cone, there is a significant stress gradient in the film. Thus, the change from a superelastic or shape memory response to plastic yield is not as well defined. For the indentation depths investigated in this paper, deformation is accommodated by both phase transformation and detwinning as well as plastic flow which results in recovery ratios significantly less than one as described by Eq. (7).

EXPERIMENTAL PROCEDURE

Ti-rich Ti-Ni thin films were deposited on silicon substrates with a 1µm ultra-low residual stress Si_3N_4 PECVD barrier layer to prevent any interaction between the film and substrate. The films were deposited at room-temperature in a magnetron sputtering system from an equiatomic NiTi target and a pure Ti target to achieve an amorphous structure. The composition of the film was determined by energy-dispersive x-ray spectroscopy (EDX) to be 51.8 at% Ti-Ni and the film thickness was 1µm. Annealing of the films was performed in a vacuum tube furnace with PID temperature control. The specimens were placed in the furnace at the annealing temperature and a slight flow of ultra-high purity Argon was maintained throughout the annealing time. The system was also evacuated using a vacuum pump after insertion of the sample to reduce the oxygen levels in the tube. To further reduce oxidation during annealing the NiTi film was placed against a small quartz plate and both pieces were enclosed in a stainless steel foil pouch. The Cr in the stainless foil oxidizes readily and removes oxygen from the atmosphere surrounding the sample.

Classical heat treatments of alloys consist of a solution treatment followed by an aging step. The solution treatment is used to homogenize the material which is then quenched to preserve its structure. The subsequent aging step is used to control the microstructure of the material. This is achieved by heating the material to a moderate temperature at which the solid solution is no longer stable, resulting in the nucleation and growth of precipitates. NiTi, however, is unable to dissolve more than 0.5 at% excess Ti at equilibrium and thus, the film used for these experiments (51.8 at% Ti-Ni) will not form a stable solid solution at any temperature [14]. Since the sputter deposited Ti-rich film has an unstable, homogeneous composition similar to a quenched solid solution, no solution treatment step was performed prior to aging. Aging treatments were performed at four different temperatures: 460, 560, 660, and 760°C and were held at those temperatures for 5, 30, and 60 minutes. After aging the samples were quenched in water to stop the precipitation process. Each aging treatment was performed on two separate samples to ensure repeatability.

Following the aging treatment the films were characterized using optical microscopy with a differential interference contrast (DIC) apparatus and heating and cooling stages. The DIC system enhances the contrast in the image through optical interference and allows for much clearer imaging of the surface of the NiTi films. Using this system, along with the heating and cooling capabilities, allows optical measurements of the phase transformation temperatures by observing the disappearance and reappearance of the martensitic surface relief upon changes in temperature.

Nanoindentation was used as a means to determine the shape memory and mechanical properties of the annealed thin films. A diamond berkovich tip, a 3-sided pyramid shape, was used to produce the indentations. Two types of indentation tests were performed on the annealed specimens. For the first type, the basic indentation test, the modulus and hardness of the films are calculated at a specified displacement into the film. By applying a small oscillating load over the basic load curve, local unloading can be achieved at each

increment in indentation depth and material properties can be measured as a function of depth into the surface. This type of test is called a continuous stiffness measurement (CSM) and is the second type of test. CSM measurements were performed to a depth of 1μm to characterize the full thickness of the film. Basic tests were performed to a depth of 100nm to minimize substrate effects on the material response. The basic indentations were subsequently imaged using an atomic force microscope to determine their initial depth, $D_{\max}$, and measured again after heating to determine the recovered depth, D_r. The recovery ratio, defined as $\Phi = (D_{\max} - D_r)/D_{\max}$, represents the level of deformation accommodated by de-twinning and phase transformations and is analogous to Eq. (7).

RESULTS AND DISCUSSION

Among the many factors that influence the mechanical and shape memory properties of NiTi films is the microstructure of the material, more specifically, the size and types of precipitates. Ti-rich NiTi has been shown to develop $NiTi_2$ precipitates; however, due to the limited solubility of Ti in NiTi, in bulk materials $NiTi_2$ precipitates only form at grain boundaries which limits their effectiveness in changing the properties of the material. Sputter deposition of Ti-rich NiTi thin films, however, is able to create an unstable structure with a homogeneous distribution of excess Ti. The subsequent aging of these films causes precipitates to form within the NiTi grains which initially form as thin-plates or GP-zones at low annealing temperatures and times [15]. These plate precipitates are coherent with the austenite matrix and their coherency strains strengthen the austenite phase. Increases in the annealing temperature or time cause the precipitates to become spherical in shape and lose their coherency with the austenite matrix resulting in a decreased critical stress for slip. Changes in the stress state and composition of the material due to precipitate formation are generally small; however, the shape memory response is very sensitive to these parameters.

Surface Relief Length

The surface relief caused by martensitic variant formation is seen clearly with the use of differential interference contrast (DIC) optical microscopy as shown in the inset images in Fig 2. This method can be used to measure the length of the martensitic plates on the surface of the sample. The length of these plates has been reported to be affected by a number of variables such as grain size and precipitation. More specifically, Zhang et al [16], have shown that martensitic plates growing in a austenitic matrix are unable to pass through the larger, spherical precipitates that form at higher temperatures and longer annealing times, but are undeterred by the smaller, coherent GP-zones that form at lower temperatures and shorter annealing times. Additionally, the high concentration of dislocations surrounding the incoherent precipitates is thought to encourage the nucleation of martensites. Thus, the films that contain only GP zones should have the longest plates which would decrease in length as the GP zones grew into spherical precipitates and by measuring the length of the martensites, the precipitate shape can be inferred.

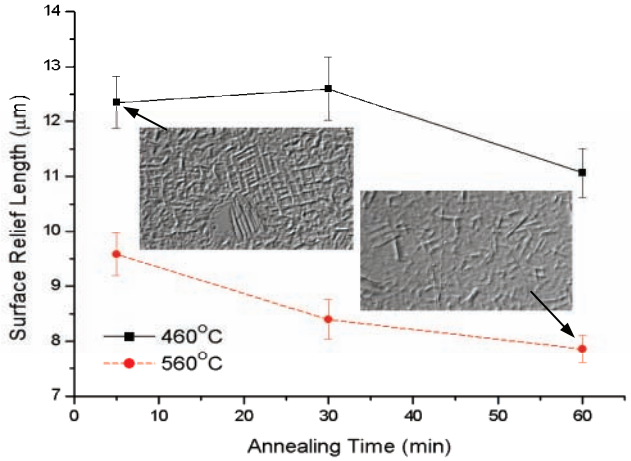

FIGURE 2: LENGTH OF MARTENSITIC SURFACE RELIEF AS A FUNCTION OF ANNEALING PARAMETERS. ERROR BARS DENOTE STANDARD ERROR. OPTICAL MICROGRAPHS INS ET

The measured martensite lengths for films annealed at 460 and 560°C are also shown in Fig. 2 as a function of time. The films annealed at 460°C, in general, have a longer surface relief length than the films annealed at 560°C. There is little change in the lengths between the samples annealed for 5 and 30 minutes at 460°C, however, the lengths begin to decrease for the 60 minute annealing time. The surface relief length for the samples annealed at 560°C are still shorter, and show a similar trend of decreasing length with annealing time. This behavior is expected due to the increase in diffusion rate at higher temperatures while longer annealing times allow for greater diffusion overall. Both of these relationships have the effect of allowing for greater growth of the precipitates from the initial GP-zones to larger spherical precipitates. As the spherical precipitates begin to form, the maximum plate length is reduced due to their inability to grow through those regions. Ishida, et al. [17] have also shown that there is a transition region between materials containing GP-zones and those with spherical precipitates where a mixture of the two types of precipitates is observed. This observation qualitatively agrees with our experimental data which shows a gradual decrease in plate length with increasing annealing temperature and time.

While precipitate formation is one factor in determining the plate size, grain size also has an effect on the maximum size due to the fact that the plates generally do not grow through grain boundaries. This suggests that a decreasing grain size could also be the reason for the observed decrease in plate length with time and temperature. However, it was observed that the maximum plate length for the films annealed at 460 and 560°C were nearly identical, suggesting that the grain size of the films is not changing significantly and thus is not responsible for the observed change in plate length. The martensitic plate length is expected to increase with further increases in annealing temperature and time due to precipitate coarsening. $NiTi_2$ precipitates have been shown to form at grain boundaries given sufficient temperature and time. This effect was not observed for the annealing parameters examined during this experiment since the films annealed at high temperatures were austenitic even upon cooling to 5°C so the surface relief could not be measured.

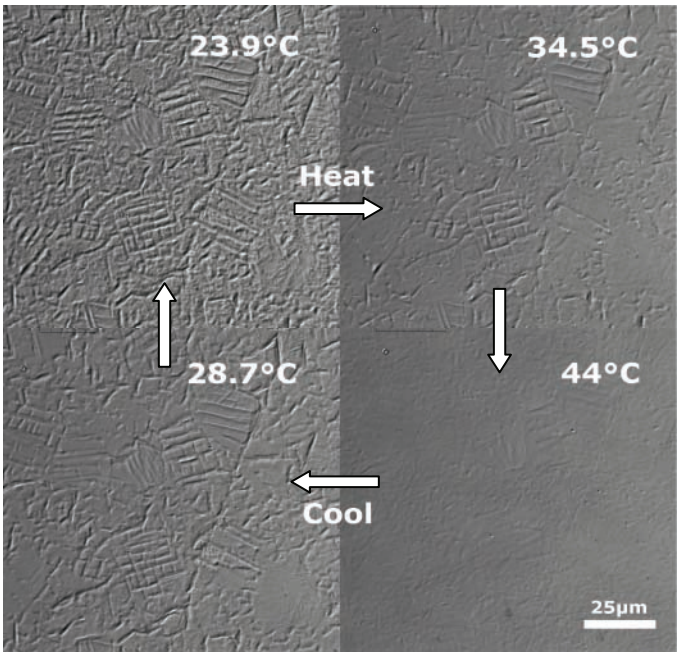

FIGURE 3: REPRESENTATIVE DIC OPTICAL MICROGRAPHS OF A MARTENSITIC SAMPLE UPON HEATING AND COOLING.

TABLE 1: TRANSFORMATION TEMPERATURES MEASURED WITH IN-SITU TEMPERATURE DEPENDENT OPTICAL MICROSCOPY

Temp (°C)	Time (min)	A_s (°C)	A_f (°C)	M_s (°C)	M_f (°C)
460	5	37.8	39.6	37.2	33.2
460	30	42.2	46.8	42.4	34.5
460	60	42.1	46.6	42.6	35.1
560	5	42.5	44.7	41.2	33.3
560	30	37.9	42.2	36.9	32.9
560	60	26.4	31	25.9	20.8
660	5	27.4	32	26.4	19.2

Transformation Temperature

The changes in surface relief of a typical martensitic specimen upon heating and cooling as observed through optical microscopy are shown in Fig. 3. This surface relief is due to the existence of various martensitic variants within the film. As the temperature is increased past the austenitic start temperature the variants begin to disappear. Upon reaching the austenitic finish temperature, the surface exhibits a smooth surface indicative of austenite. Upon cooling from the elevated temperature, the variants begin to reappear at the martensitic start temperature, and have fully developed upon reaching the martensitic finish temperature. By tracking the temperature of the sample and observing the appearance and disappearance of the martensitic variants, a measure of the transformation temperatures of the film can be obtained. Transformation temperatures of films obtained using this method are shown in Table 1. Not all samples are included in Table 1 since some samples did not undergo any visible transformation even when cooled to 5°C, the limit of the cooling stage used in this

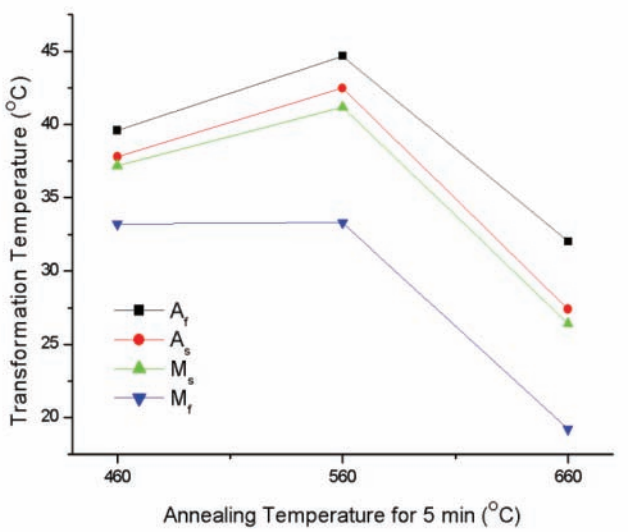

FIGURE 4: TRANSFORMATION TEMPERATURES VS ANNEALING TEMPERATURE FOR FILMS ANNEALED FOR 5 MINUTES

experiment. All samples where this was the case were annealed at temperatures above 660°C. This is evidence of a significant drop in transformation temperatures of the surface of the films when annealing is performed at elevated temperatures.

The effect of annealing temperature on the transformation temperatures for samples annealed for 5 minutes is shown in Fig. 4. This trend of decreasing transformation temperatures with increasing annealing temperature is attributed to the change in matrix composition and was observed for longer annealing times as well (not shown). The effect of annealing time on the transformation temperatures of samples annealed at 560°C is depicted in Fig. 5 and also shows a decreasing trend. It has been reported [18] that the transformation temperatures of NiTi are a strong function of composition with Ti-rich samples having higher transformation temperatures and decreasing with decreasing Ti content. Since the solubility limit of Ti in NiTi is nearly constant with temperature, the driving force for diffusion for all annealing parameters is similar. Increased annealing time and temperature allow for greater diffusion within the Ti-rich samples which leads to greater precipitation and thus a decrease in the Ti content of the matrix which is accompanied by the observed decrease in transformation temperatures. The transformation temperatures of samples annealed at 460°C, however, were nearly constant with annealing time, suggesting that the diffusion rate at this temperature is too low to have a significant effect on the matrix composition.

It should also be noted that for the annealing parameters considered in this study, the precipitate shape and size does not seem to have a significant effect on the transformation temperatures of the samples. Ishida et al. [19] have reported significant increases in the transformation temperatures of Ti-rich NiTi thin films with annealing time.

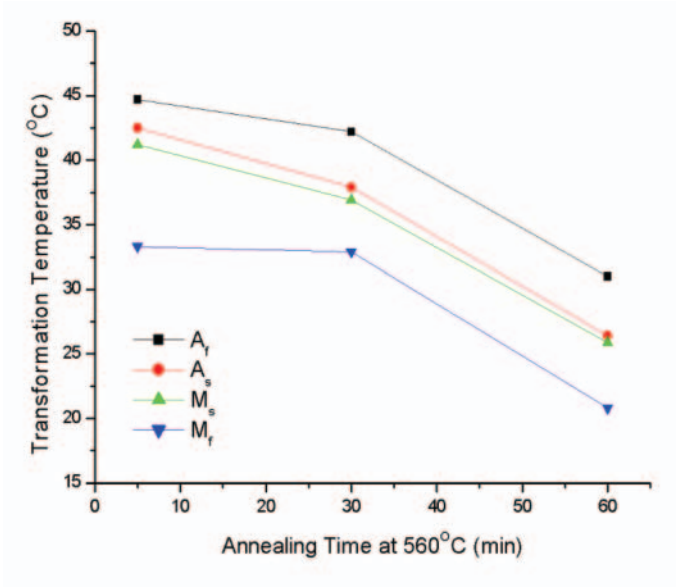

FIGURE 5: TRANSFORMATION TEMPERATURES VS ANN EALING TIME FOR FILMS ANNEALED AT 560°C.

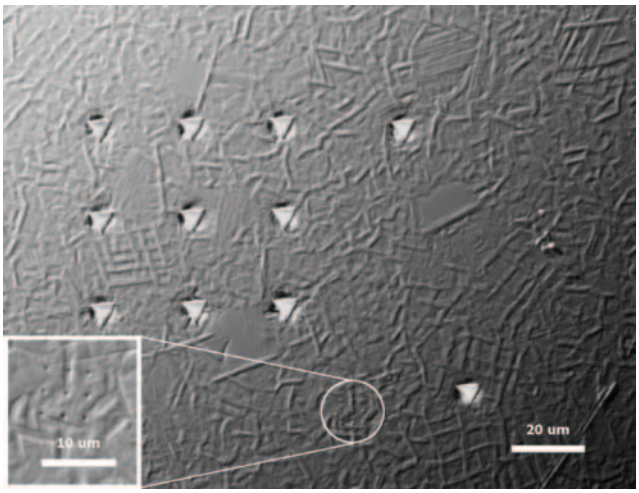

FIGURE 6: OPTICAL MICROGRAPH OF RESIDUAL IMPRE SSIONS FROM 1μm AND 100nm (INSET) DEEP INDENTATI ONS ON ANNEALED NITI FILM BEFORE HEATING. FILM A NNEALED AT 460°C FOR 5 MINUTES

However, their experiments were performed for much longer times, from 1 hour to 100 hours, and only spherical $NiTi_2$ precipitates were observed. Initial diffusion and precipitation rates are high due to the insolubility of excess Ti and are expected to decrease with time and cause the matrix Ti composition to decrease quickly at first. Thus, as observed, the effect of matrix composition should be stronger for shorter annealing times and have less of an effect for extended heat treatments.

Mechanical Response

As described previously, the transformation temperatures of SMAs have a significant effect on their response to loading. Depending on the initial structure of the film, the deformation induced by the indenter can be accommodated by different mechanisms. Films that are martensite at room temperature accommodate the indentation through elastic deformation of the martensite, de-twinning, and plastic deformation of the martensite. The residual imprint left in the sample after the tip is retracted is the deformation accommodated by de-twinning and plasticity. Films that are austenitic at room temperature accommodate the deformation initially by elastic deformation of the austenite, the stress induced phase transformation to martensite, followed by elastic and plastic deformation of the martensite. Plastic deformation of the austenite can also be induced depending on the level of stress required to cause the austenite to martensite phase transformation. For these films, the residual imprint is the deformation accommodated by plasticity of the austenite or martensite and any residual stress-induced martensite left after unloading. Upon heating, martensitic films will transform to austenite, recovering the deformation accommodated through de-twinning while austenitic films may recover some deformation through transformation of residual stress-induced martensite.

Figure 6 is an optical micrograph of indentations made in a martensitic film which was annealed at 460°C for 5 minutes. The larger 3x3 array is a set of 1μm deep CSM indentations, while the smaller array (inset) consists of nine, 100nm deep basic indents. The reference indentations are used to aid in locating the arrays under optical microscopy and AFM. The CSM indentations are spaced 25μm apart and the basic indentations 300nm apart to minimize the effect of adjacent tests on the mechanical response. Surface relief typical of martensite is also visible over the entire film surface. Upon heating of the specimen, recovery of the 100nm indentations was observed optically, however, recovery of the CSM indentations was not apparent due to the level of plasticity involved.

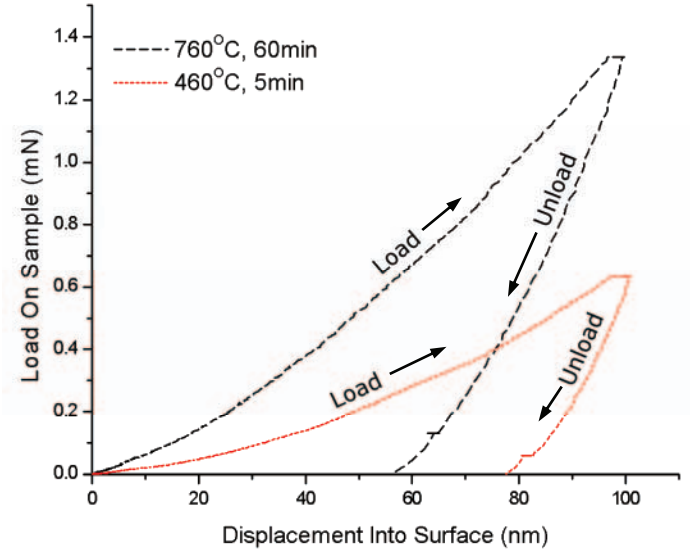

FIGURE 7: REPRESENTATIVE LOAD-DISPLACEMENT CURV ES FOR 100nm INDENTATION IN ANNEALED FILMS. NOTE SMALLER RESIDUAL INDENTATION DEPTH OF AUSTENITI C FILM DUE TO SUPERELASTICITY

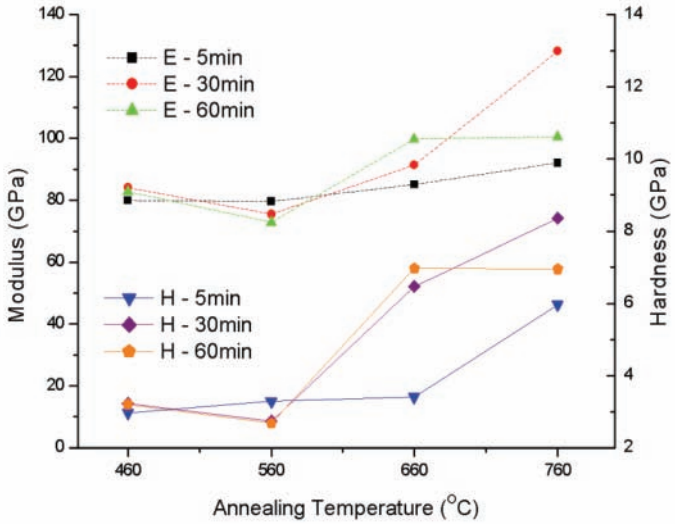

FIGURE 8: MODULUS AND HARDNESS OF FILMS ANNEALED AT VARIOUS TEMPERATURES AND TIMES

Figure 7 shows representative load-displacement curves for 100nm basic indentations into martensitic and austenitic films. Arrays of both 100nm basic and 1μm CSM indentation tests were performed on all samples. The resulting modulus and hardness of the films as a function of annealing temperature are shown in Fig. 8. An increase in both modulus and hardness with annealing temperature is observed for all annealing times and is due to the decrease in transformation temperatures with annealing time. As the forward transformation temperatures drop below room temperature, the room temperature phase changes from martensite to austenite. The presence of austenite, a stiffer and harder phase, results in the observed changes.

Aside from the modulus and hardness of the films, a number of additional parameters of interest can be calculated directly from the load-displacement curves. The displacement at zero load on the unloading curve gives a measure of the indentation depth remaining in the surface after removal of the indenter tip. This value is much smaller for austenitic films than martensitic ones due to the pseudo-elastic deformation accommodate by the phase transformation. The reverse transformation from martensite to austenite, which occurs in the course of unloading for austenitic films, allows the films to recover a greater amount of the induced deformation prior to heating.

Additionally, the area within the load-unload curves represents the energy dissipated during the indentation. This value can be used to determine the dissipated energy ratio which is defined as the dissipated energy divided by the total energy input, the area under the loading curve. For a martensitic film, energy dissipation is caused by plastic deformation as well as de-twinning. For an austenitic film, energy dissipation is caused solely by plastic deformation since any deformation accommodated by phase transformation is recoverable upon unloading.

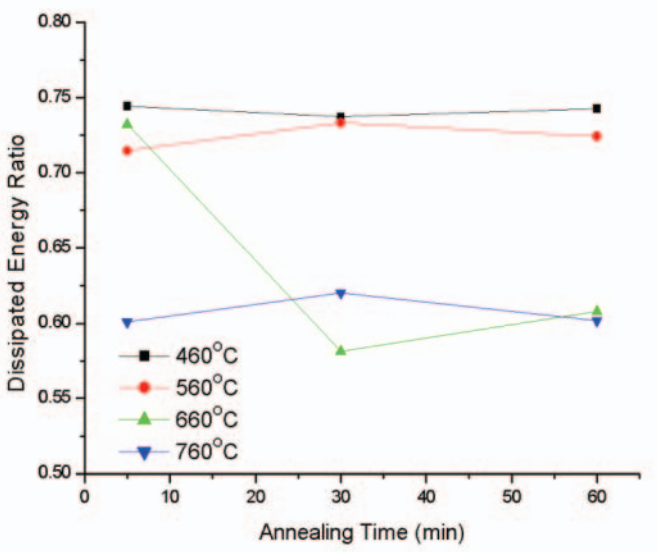

FIGURE 9: DISSIPATED ENERGY RATIO VS ANNEALING TIME AT VARIOUS TEMPERATURES. NOTE REDUCED DISSIPATION FOR HIGHER TEMPERATURE HEAT TREATMENTS DUE TO AUSTENITIC STRUCTURE

The dissipated energy ratio for films annealed at various temperatures is shown in Fig. 9. The films annealed at lower temperatures, 460 and 560°C, show a large dissipated energy ratio of about 0.75. As the annealing temperature is increased, the dissipated energy ratio drops to near 0.6. This drop is also due to the change in transformation temperatures of the films. Since more energy is recovered in austenitic films due to the superelastic effect, they are expected to dissipate less energy during indentation. However, not all of the samples annealed at 660°C exhibit the low dissipated energy ratio. The sample annealed for 5 minutes shows a ratio indistinguishable from the films annealed at 460 and 560°C. This is also the only film annealed above 560°C that shows any martensite at room temperature. Thus, the dissipated energy ratio is directly related to the room temperature phase of the material and is nearly constant for each phase with a step change in between.

Recoverable Depth

In addition to the material and shape memory properties derived from the indentation load-displacement curves, further characterization of the films can be achieved through a coupled nanoindentation-AFM experiment. The recoverable depth of indentation is a measure of the available shape memory material within the film. Residual indentation depth in martensitic films can be caused to recover through the shape memory effect by heating the films above their austenitic start temperatures with full recovery achieved by heating the films above their austenitic finish temperatures. Measurements of the indentation depths before and after heating are used to calculate the depth recovery ratio for the films. Cross-section AFM scans of an indentation in a martensitic film before and after heating are shown in Fig. 10 and show clear depth recovery.

Figure 11 shows the effect of annealing temperature on the depth recovery ratio of films annealed for 5 minutes. A clear

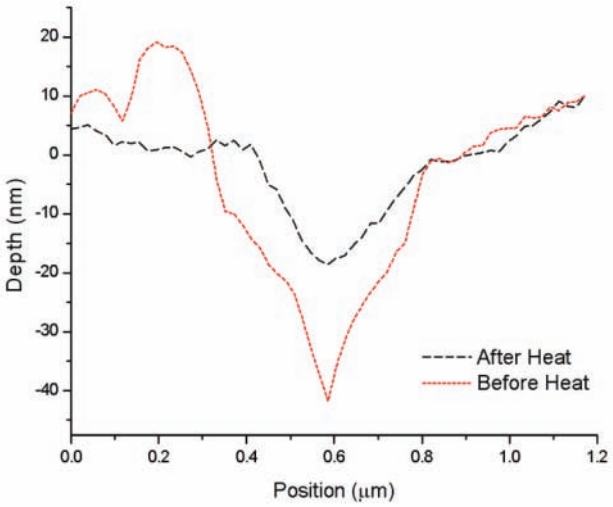

FIGURE 10: CROSS-SECTION OF TYPICAL AFM SCAN OF INDENTATIONS IN A MARTENSITIC FILMS BEFORE AND AFTER HEATING SHOWING DEPTH RECOVERY. FILM AN NEALED AT 460°C FOR 5 MINUTES

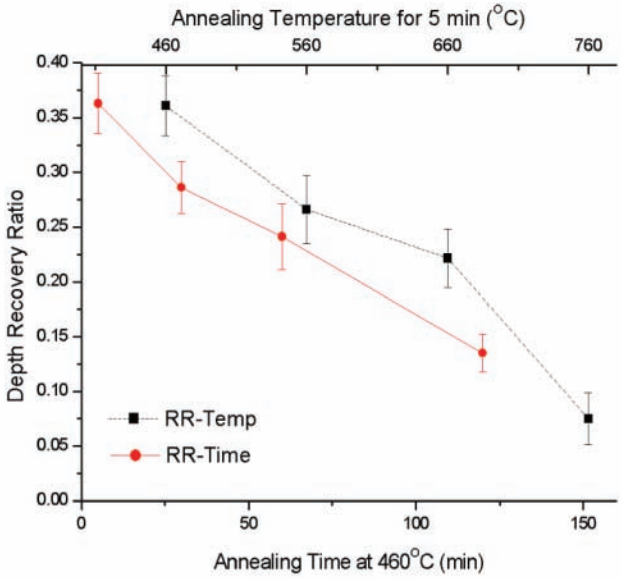

FIGURE 11:RECOVERY RATIO AS A FUNCTION OF ANNE ALING TEMPERATURE AND TIME. ERROR BARS DENOTE STANDARD ERROR

downward trend in recovery ratio is seen with increasing annealing temperature. This trend is due to a combination of effects including the shift in transformation temperatures as well as the change in precipitate shape as described in previous sections. Annealing at 460°C produces a fully crystalline, fully martensitic film with GP-zones rather than spherical precipitates. This combination produces the greatest level of depth recovery upon heating since the entire film is viable shape memory material and since GP-zones have been shown to inhibit plastic deformation. Thus the film is able to accommodate large transformation strains before reaching plasticity.

As shown in previous sections, as the annealing temperature of the films is increased a drop in transformation temperatures and a transition toward larger, spherical precipitates is observed. A decrease in transformation temperatures can have the effect of increasing the critical stress for inducing martensite as depicted in Fig. 1, however, for films that are martensitic at room temperature, this effect is very small and is not expected to have a significant effect on the change in recovery ratio between the films annealed at 460 and 560°C. The presence of austenite in films annealed at higher temperatures, 660 and 760°C, contributes to the reduced recovery ratio observed. The austenite in the films is not viable for the shape memory effect at room temperature and thus cannot contribute to the recovery of the indentation depth upon heating. In addition, the increase in the critical stress for phase transformation with decreasing transformation temperatures for the austenitic films could have the effect of increasing the amount of plasticity.

The reduced recovery experienced by the film annealed at 560°C is attributed to the transition from GP-zones to spherical precipitates which have been shown to allow for greater plastic deformation. Considering Eq. 7, the decrease in recovery ratio at this temperature is due to a decrease in Y_{pl} rather than an increase in Y_{mr}. The further decrease in depth recovery for the 660 and 760°C cases is attributed primarily to the increase in Y_{mr}. The forward transformation temperatures of the 660°C sample are close to room temperature which suggests a low stress to induce the phase transformation. The 760°C sample, however, did not transform even when cooled to 5°C. This suggests a significantly higher critical stress for transformation as expressed by Eq. 3. The dependence on $\underline{Y_{pl}}$ for lower temperature anneals and Y_{mr} for higher temperature anneals agrees qualitatively with the observations by Kajiwara et al [15] that the critical stress for slip in sputtered Ti-rich NiTi films is a decreasing function of heat treatment temperature up to 820K and is nearly constant above that temperature.

The fractions of the induced deformation accommodated by the different mechanisms in each sample are shown in Fig. 12. As expected, amongst the martensitic films, the 560°C samples show greater plastic deformation than the 460°C samples while amongst the austenitic films, the 760°C samples shows greater plastic deformation than the 660°C samples due to the increase in Y_{mr}. Overall, the thermally induced recovery decreases with annealing temperature due to the change in the room temperature phase from martensite to austenite. The elastic and superelastic deformation increases for the 660°C case due to the added deformation accommodated by superelasticity.

The effect of annealing time on the depth recovery ratio is also shown in Fig. 11 for films annealed at 460°C and shows a trend of decreasing depth recovery with increasing annealing time. In this case, however, all of the films are martensite at room temperature.

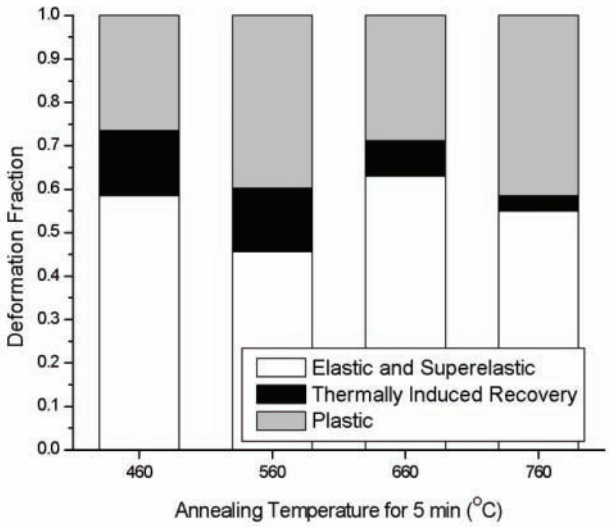

FIGURE 12: PERCENTAGE OF DEFORMATION ACCOMMO DATED BY DIFFERENT MECHANISMS FOR FILMS ANNEA LED FOR 5 MINUTES

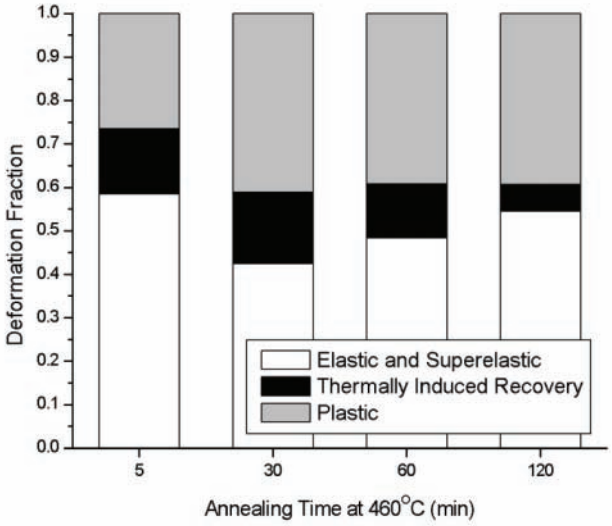

FIGURE 13: PERCENTAGE OF INDENTATION DEFORMATI ON ACCOMMODATED BY DIFFERENT MECHANISMS AS A FUNCTION OF ANNEALING TIME AT 460°C.

Thus, the stress required for phase transformation and the percentage of viable shape memory material in the films are not expected to differ significantly between samples and should have little effect on the recovery ratio. Rather, the decrease in recovery ratio with annealing time is due to the effects of the precipitates within the grains. As shown previously, films annealed at 460°C start with GP-zones for short annealing times and transition toward the larger spherical $NiTi_2$ precipitates for longer annealing times. The strengthening effect of the GP-zones increases the critical stress for slip which results in larger depth recovery. As the films transition toward spherical precipitates this strengthening effect lessens, decreasing Y_{pl} and reducing the depth recovery.

The fractions of the induced deformation accommodated by the different mechanisms for the samples annealed at 460°C are shown in Fig 13. The low level of plastic deformation is clearly seen for the film annealed for 5 minutes due to strengthening by the GP-zones. The level of plastic deformation is nearly constant for annealing times beyond 5 minutes, however, the level of thermally induced recovery begins to decrease. This decrease in thermally induced recovery could be attributed to increased Y_{mr} due to limited growth of martensitic variants in films with spherical precipitates.

Similar trends were observed for films annealed at 660 and 760°C as a function of time and for films annealed for 30 and 60 minutes as a function of temperature (not shown). With overall decreases in the transformation temperatures with increasing annealing time and temperature, the stress required to induce the transformation keeps increasing. This results in first, a transition between shape memory and superelastic responses, and second, increases in the level of plasticity experienced by the films and decreases in the depth recovery ratio. Films annealed at 560°C did show a slightly higher level of depth recovery than the films annealed at 460°C. It is possible that the precipitates in these films produce the greatest strengthening and thus the highest recovery, however, this area requires further investigation. Films annealed at 660°C and above showed negligible depth recovery upon heating since they are primarily austenite at room temperature.

CONCLUSION

The effects of heat treatment temperature and time on the resulting mechanical and shape memory properties of Ti-rich, amorphous NiTi films have been examined. The heat treatments resulted in both martensitic and austenitic films for different annealing parameters which demonstrates a significant shift in the transformation temperatures of the material. Control over the transformation temperature would allow for shape memory devices to be activated at different temperatures for use in different thermal environments, or to control whether shape memory or superelastic characteristics will be exhibited. Transformation temperatures have been shown to decrease as a function of heat treatment time and temperature which is attributed to the development of GP-zones and spherical precipitates within the NiTi grains and the corresponding decrease in the Ti-content of the matrix. It has also been observed that matrix composition has a more significant effect than precipitate size and distribution for the shorter heat treatments performed in this study. The mechanical response of films under indentation revealed increases in the critical stress for slip for films containing GP-zones as well as a step decrease in dissipated energy between martensitic and austenitic films. The recovery ratio after indentation was also shown to vary with annealing parameters. Larger critical stresses for slip and larger recovery ratios would enable devices to accommodate larger recoverable deformations for actuation applications. The results described above demonstrate that short term aging treatments are a viable mechanism to tailor the mechanical and shape memory response of amorphous Ti-rich NiTi films.

REFERENCES

[1] Bellouard, Y., 2008, "Shape memory alloys for Microsystems: A review from a material research perspective", Materials Science and Engineering A, **481-482**, pp. 582-589.

[2] Ishida, A., Takei, A., Miyazaki, S., 1993, "Shape memory thin film of Ti-Ni formed by sputtering", Thin Solid Films, **228**, pp. 210-214

[3] Lee, H., Ni, H., Wu, D.T., Ramirez, A.G., 2005, "Grain size esitmations from the direct measurement of nucleation and growth", Applied Physics Letters, **87**, pp. 124102-1-3

[4] Paula, A.S., Canejo, J.P.H.G., Martins, R.M.S., Fernandes, B., 2004, "Effect of thermal cycling on the transformation temperature ranges of a Ni-Ti shape memory alloy", Materials Science and Engineering A, **378**, pp. 92-96

[5] Ishida, A., Sato, M., Miyazaki, S., 1999, "Mechanical properties of Ti-Ni shape memory thin films formed by sputtering", Materials Science and Engineering A, **273-275**, pp. 754-757

[6] Firstov, G.S., Vitchev, R.G., Kumar, H., Blanpain, B., Van Humbeeck, J., 2002, "Surface oxidation of NiTi shape memory alloy", Biomaterials, **23**, pp. 4863-4871

[7] Gall, K., Dunn, M.L., Liu, Y., Sehitoglu, H., Chumlyakov, Y.I., 2002, "Micro and macro deformation of single crystal NiTi", Transactions of the ASME, **124**, pp. 238-245

[8] Tall, P.D., Ndiaye, S., Beye, A.C., Zong, Z., Soboyejo, W.O., Lee, H., Ramirez, A.G., Rajan, K., 2007, "Nanoindentation of Ni-Ti thin films", Materials and Manufacturing Processes, **22**, pp. 175-179

[9] Shaw, G.A., Crone, W.C., 2004, "Direct measurement of the nanoscale mechanical properties of NiTi shape memory alloy", in Materials Research Society Symposium Proceedings: Mechanical Properties of Nanostructured Materials and Nonocomposites, **791**, Boston, USA, pp. 215-220

[10] Shimizu, K., Tadaki, T., 1987, Shape memory effect: mechanism, in H. Funakubo (ed) Shape Memory Alloys, Gordon and Breach Science Publishers, 1-60.

[11] Hill, R., 1950, *The Mathematical Theory of Elasticity*, Oxford University Press, Oxford, pp. 97-101, Chap. 5.

[12] Johnson, K.L., 1985, *Contact Mechanics*, Cambridge University Press, Cambridge, pp. 171-175, Chap. 6.

[13] Shaw, G.A., Stone, D.S., Johnson, A.D., Ellis, A.B., Crone, W.C., 2003, "Shape memory effect in nanoindentation of nickel-titanium thin films", Applied Physics Letters, **83**(2), pp. 257-259.

[14] Murray, J.L., 1991, "Ni-Ti (Nickel-Titanium)", *Phase Diagrams of Binary Nickel Alloys*, P. Nash ed., ASM International, Materials Park, OH, pp. 342-355.

[15] Kajiwara, S., Kikuchi, T., Ogawa, K., Matsunaga, T., Miyazaki, S., 1996, "Strengthening of Ti-Ni shape-memory films by coherent subnanometric plate precipitates", Philosophical Magazine Letters, **74**, pp. 137-144

[16] Zhang, Z.X., Sato, M., Ishida, A., 2002, "Influence of Guinier-Preston zones on deformation in Ti-rich Ti-Ni thin films", Philosophical Magazine Letters, **82**(5), pp. 257-264.

[17] Ishida, A., Sato, M., Kimura, T., Sawaguchi, T., 2001, "Effects of Composition and Annealing on Shape Memory Behavior of Ti-rich Ti-Ni Thin Films Formed by Sputtering", Materials Transactions, **42**(6), pp. 1060-1067.

[18] Eckelmeyer, K.H., 1976, "The Effect of Alloying on the Shape Memory Phenomenon in Nitinol", Scripta Metallurgica, **10**, pp. 667-672.

[19] Ishida, A., Sato, M., Takei, A. & Miyazaki, S. (1995) Effect of heat treatment on shape memory behavior of Ti-rich Ti-Ni thin films, Materials Transactions JIM 36, 1349-1355